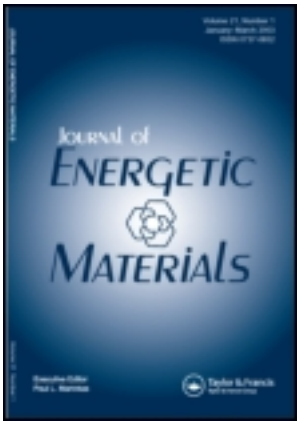

Journal of Energetic Materials
Publication details, including instructions for authors and subscription information:
http://www.tandfonline.com/loi/uegm20

Synthesis and Reactive Properties of Iron Oxide-Coated Nanoaluminum

Daniel A. Kaplowitz [a], Guoqiang Jian [a], Karen Gaskell [a], Rohit Jacob [a] & Michael R. Zachariah [a]
[a] Department of Chemical and Biomolecular Engineering, University of Maryland, College Park, Maryland
Published online: 11 Sep 2013.

To cite this article: Daniel A. Kaplowitz, Guoqiang Jian, Karen Gaskell, Rohit Jacob & Michael R. Zachariah (2014) Synthesis and Reactive Properties of Iron Oxide-Coated Nanoaluminum, Journal of Energetic Materials, 32:2, 95-105, DOI: 10.1080/07370652.2013.767288

To link to this article: http://dx.doi.org/10.1080/07370652.2013.767288

Journal of Energetic Materials, 32: 95–105, 2014

ISSN: 0737-0652 print/1545-8822 online
DOI: 10.1080/07370652.2013.767288

Synthesis and Reactive Properties of Iron Oxide–Coated Nanoaluminum

DANIEL A. KAPLOWITZ, GUOQIANG JIAN, KAREN GASKELL, ROHIT JACOB, AND MICHAEL R. ZACHARIAH

Department of Chemical and Biomolecular Engineering, University of Maryland, College Park, Maryland

A homogeneous coating of Fe_3O_4 on in situ–generated nanoaluminum was accomplished by thermal decomposition of $Fe(CO)_5$ in an aluminum aerosol stream and subsequent oxidation of iron by air bleed. X-ray photoelectron spectroscopy (XPS) investigation revealed that oxygen penetrated through this coating, and Fe_3O_4 facilitated the formation of an expanded aluminum oxide layer compared to an uncoated aluminum case. Closed cell combustion tests displayed a minor decrease in pressure response for the coated product, which was attributed to the increased aluminum oxide layer. The critical ignition temperature was reduced for the coated product in T-jump fine-wire combustion tests.

Keywords aerosol; ignition temperature; iron (II, III) oxide; iron oxide–coated nanoaluminum; iron pentacarbonyl

Introduction

Nanoaluminum is the primary nanostructured component in nanoenergetic formulations. Though a variety of nanoscale oxidizers are employed, the fuel is almost exclusively aluminum because of its ready availability and reactive properties. Piercey and Klapotke have reviewed nanoscale aluminum thermite reactions, detailing how tailored preparation methods can allow their use to replace conventional energetic materials for certain military and civilian applications [1]. One of the concerns that has developed in the use of nanoaluminum is the 2- to 5-nm native oxide that naturally forms when exposed to any moisture or air. Any aluminum will form such an oxide layer, which for micrometer-size particles accounts for only a small fraction of the mass of the particle. However, as the particle size decreases into the nano regime, this oxide coating can represent a large fraction of the particle's mass. For example, a 100-nm particle containing a 5-nm alumina shell will contain 20% of the particle's total mass as aluminum oxide. As the particle size decreases further, this percentage increases drastically. Thus, only a small amount of material is actually available for a desired energetic process. Furthermore, this alumina coating causes significant impedance for reaction due to its high melting

Address correspondence to Michael R. Zachariah, University of Maryland, Department of Mechanical Engineering, Campus Drive, 2125 Martin Hall, College Park, MD 20742, USA. E-mail: mrz@umd.edu

point of 2072°C compared to aluminum's melting point of 660°C. The shell is essentially a nonreactive material, so in order to react the aluminum core must either escape the shell or oxidizer must diffuse through. This suggests the possibility of another type of coating that might either enhance aluminum transport/reactivity or itself have higher fuel content. In this study we focus on the former approach.

The most common approach to preventing surface oxidation of aluminum is to develop a coating before oxidation can occur. A nonreactive passivation layer used for storage can be removed when the aluminum is needed. Hammerstroem et al. were able to develop nonpyrophoric unpassivated nanoaluminum by polymerizing epoxides on the particle surface in solution [2]. A more potentially valuable application, however, is a functional energetic material coating that can directly react with the aluminum core during combustion. A functional coating on bare aluminum can not only prevent the oxide layer from forming but can also affect agglomeration during processing and alter the energy release mechanisms during combustion. If one could directly attach an oxidizer to an aluminum surface in such a manner as to prevent spontaneous runaway reaction, one could potentially have a structure with higher energy content on a mass basis, with the potential of favorably altered kinetics.

Functional coatings on aluminum have been successfully developed by Jouet et al. with a perfluorocarboxylic acid in solution [3]. They were able to prevent oxidation of the aluminum by forming a self-assembled monolayer of the acid on the particle surface, thus enhancing the reactivity of the system. Unfortunately, issues arose with production of bulk material for this case due to the highly pyrophoric nature of this material without the presence of the aluminum oxide layer. Horn et al. prepared a similar perfluorocarboxylic acid coating on the particle surface on top of the aluminum oxide layer present and demonstrated via flame tests that even without passivation, energetic enhancement can still be achieved from direct oxidizer delivery in a nanoparticle coating [4].

Metals can also be used for coating bare nanoaluminum to improve energetic function. Iron has successfully been coated on the surface of micrometer-sized aluminum particles by chemical precipitation methods. These particles have shown decreased agglomeration, thus increasing their efficiency. The premise behind this phenomenon, demonstrated by Breiter et al., is that increasing the surface metal melting temperature above the combustion temperature yields a significant decrease in agglomeration during a combustion event [5]. Because Fe has a much higher melting temperature than Al, 1538°C compared to 660°C, a coating allows for less agglomeration when burning and therefore a more efficient material. Burn tube experiments with this product showed a significant enhancement in flame speed compared to untreated aluminum. Metal-coated aluminum particles have also exhibited decreased critical ignition temperatures, theorized by Shafirovich et al. to be due to exothermic alloying reactions [6]. Andrzejak et al. found evidence of this Al-Fe alloying for millimeter-sized iron-coated aluminum particles that resulted in significantly lowered ignition temperatures during laser combustion experiments [7].

For a nanoscale coating, however, it is unlikely for a 1- to 3-nm layer to remain in the elemental state upon exposure to air due to the highly pyrophoric nature of iron. Most likely a thin coating of iron would react with oxygen, resulting in an iron oxide layer on the aluminum surface. Work by La et al. has shown that for appropriate powder mixing stoichiometries, iron oxide and aluminum can react to form Fe_3Al according to the reaction shown in Eq. (1) [8]:

$$3Fe_2O_3 + 8Al \rightarrow 2Fe_3Al + 3Al_2O_3 \quad \Delta H^o_{f,298K} = -2550\text{kJ} \cdot \text{mol}^{-1}. \qquad (1)$$

The energy released from this exothermic reaction could alter combustion characteristics in a thermite reaction with a thin layer of iron oxide coated on the aluminum surface.

Because commercially available aluminum necessarily already has a native oxide coating, we need to first create nanoaluminum in a nonoxidizing environment and then proceed to passivate the particle on the fly. In a prior work we developed a low-temperature gas-phase scheme that uses triisobutylaluminum (TibAl) as a metal organic precursor, which when decomposed in the gas phase at 350°C produces an aerosol of highly faceted crystals of aluminum [9]. Particles grow into a polyhedral morphology with an average diagonal distance of ~90 nm. Production was accomplished under argon gas, thus allowing formation of a bare aluminum surface. The in-line aerosol process lends itself well to combination with coating systems for passivation. Without such a coating, the exposed aluminum forms a 5-nm oxide layer.

In order to develop a coating of iron oxide on our aluminum particles to explore its potential to passivate and functionalize the surface, an appropriate iron production method had to be selected. A subsequent air bleed after coating will allow the iron to react to form the oxide. Current techniques for iron via chemical methods in solution include microemulsions [10], chemical coprecipitation [11], liquid-phase reduction [12], and electrodeposition [13]. These batch methods, though dependable, are not easily incorporated in an aerosol system for continuous flow.

Gas-phase reduction can be accomplished by heat-reducing iron ores such as goethite or hematite with hydrogen gas [14], but a simpler gas-phase process has been shown via decomposition of iron pentacarbonyl and subsequent chemical vapor condensation of iron [15,16]. Such chemical vapor condensation experiments have shown thermal pyrolysis of iron pentacarbonyl at relatively low temperatures to form iron particles and a gaseous by-product CO. The inherent aerosol process lends itself to coupling with our Al scheme for a coating. These details combined with our previous experience with the technology led to its selection for iron production.

Experimental Setup

The basic experimental configuration is shown in Fig. 1. The bare aluminum production technique developed previously [9] involves bubbling of argon through 60°C heated triisobutylaluminum precursor with a partial pressure of 3.3 mmHg

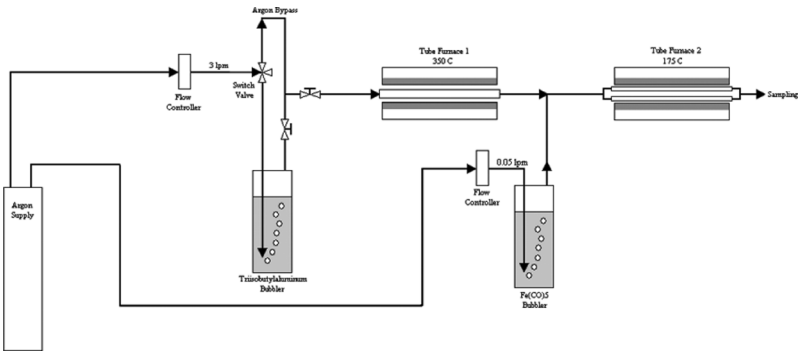

Figure 1. Experimental setup for iron oxide coating of aluminum via pyrolysis of iron pentacarbonyl.

and subsequent thermal pyrolysis at 350°C in a total flow of 3,000 sccm. This aerosol system was coupled with an adapted chemical vapor condensation experiment for thermal decomposition of iron pentacarbonyl. The final iron production setup consisted of a glass bubbler filled with 25 mL of $Fe(CO)_5$ through which flow-metered argon was passed at a rate of 50 sccm. Due to the high vapor pressure of the liquid at room temperature, it was not necessary to heat the precursor, resulting in an $Fe(CO)_5$ partial pressure of 28.3 mmHg in argon. This product was combined with the aluminum nanoparticle aerosol consisting of an aluminum total mass flow of 1.3 E-2 g/min and passed to a 15.5-in. tube furnace with a residence time of 1.8 s at 175°C to decompose the iron precursor and minimize any alloying reactions with the aluminum.

Due to concerns with iron pentacarbonyl toxicity, all downstream lines were completely flushed with argon after collection of the product. The addition of multiple three-way Swagelok valves and purge lines allowed for proper ventilation but is not shown in Fig. 1. Due to the pyrophoric nature of the iron coating, following collection of the material a slow bleed of a lean air/argon mix was sent through the product while heating the holder to 50°C with heating tapes to allow for passivation of product to yield the iron oxide coating.

Results and Discussion

Product Analysis

Final conditions for iron oxide coating employed a decomposition furnace temperature of 175°C with an outlet flow of 4.3 E-3 g/min Fe for 100% theoretical precursor conversion combined with the aluminum aerosol mass flow of 1.3 E-2 g/min, resulting in a 0.33 value for Fe/Al mass ratio. The Fe/Al mass ratio corresponds to a theoretical iron oxide coating of 6.4 nm on a 90-nm Al particle for 100% condensation of iron onto the particle surface. The low vapor concentration of iron should promote homogeneous condensation over heterogeneous nucleation.

To obtain a coating thickness based on experimental production of iron, we require knowledge of the particle size distributions for both the aluminum and the iron material, which we obtain separately using a scanning mobility particle size system composed of a differential mobility analyzer coupled with a condensation particle counter, an experimental system detailed elsewhere [17].

Size measurements were fitted to lognormal distributions for the plots in Fig. 2. Because these measurements do not account for aggregation of particles, adjusted

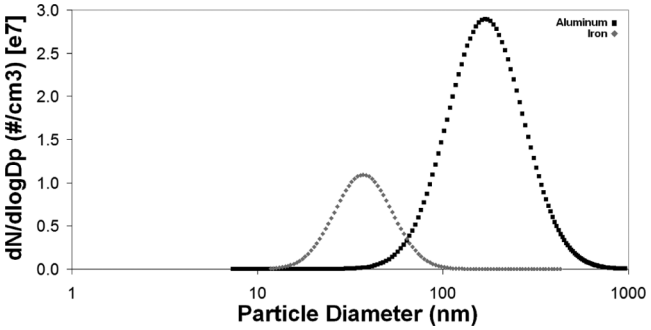

Figure 2. Lognormal-fitted particle size distributions for iron and aluminum.

calculations are required based on these distributions, accomplished with a scaling factor and use of primary particle sizes for aluminum and iron as measured from transmission electron microscopy (TEM) imaging. Assuming a 100% condensation of iron onto the aluminum nanoparticle surface, we can estimate the coating thickness on the aluminum core. Pure iron particle measurements are converted into an iron oxide basis, and iron oxide thickness can be determined. The mass ratio of Al to Fe based on these experimental results gives a value of 0.29, resulting in a coating thickness of 5.75 nm Fe_3O_4. The slight difference between the theoretical coating thickness and calculations based on experimental size distributions can be attributed to deposition of iron carbonyl precursor to the tube walls.

Product collected from the iron coating system was passivated with air to form iron oxide, and once a stable sample was obtained it was examined using the University of Maryland NISPLab JEOL JEM 2100F TEM/STEM. An example of TEM imaging of product particles with the coating is show in Fig. 3. The TEM clearly shows an ~5-nm amorphous conformal coating on the aluminum particle.

To determine the chemical nature of the coating, energy-dispersive X-ray spectroscopy (EDS) characterization was performed, and the results shown in Fig. 4 clearly indicate that the shell on the aluminum does in fact contain iron and oxygen. Because high-resolution imaging showed that the shell was amorphous, it is likely that the iron coating had oxidized completely during the air bleed to form a homogenous iron oxide coating. Due to minor image shifting during measurements, EDS line scan plots cannot be used for direct quantification of iron oxide coating thickness but only to confirm the presence of iron at the edge of the particle.

The presence of iron, oxygen, and aluminum at the edge of the particle could indicate the development of a mixed metal oxide phase such as $FeAl_2O_4$ hercynite or an amorphous coating of composition proportional to $FeO \cdot Al_2O_3$. Because high-resolution TEM demonstrated that the coating was completely amorphous, we can rule out the presence of any crystalline hercynite. To further evaluate the composition of the amorphous layer on the aluminum surface to establish the phase of iron oxide or a potential mixed metal oxide, X-ray photoelectron spectroscopy (XPS) results for the aluminum and iron phases are shown in Figs. 5 and 6, respectively. This gives a local characterization of the edge of the particle by analysis of electrons expelled from the top 1 to 10 nm of the particle during irradiation, with this penetration distance largely depending on the density of the material.

Figure 5 demonstrates unambiguously that aluminum oxide has formed on the surface of the aluminum core despite the iron oxide coating. It is clear that the iron oxide coating either did not act as a passivation layer or the iron oxide itself continuously reacted with the underlying aluminum. The aluminum oxide peak matches well

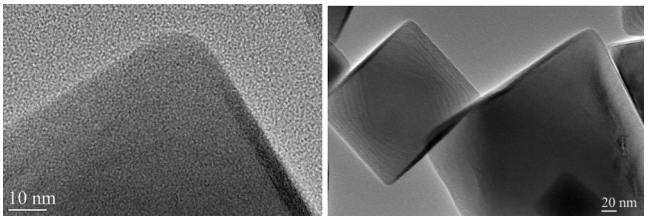

Figure 3. High-resolution TEM images of polyhedral particles from the iron oxide coating experiment.

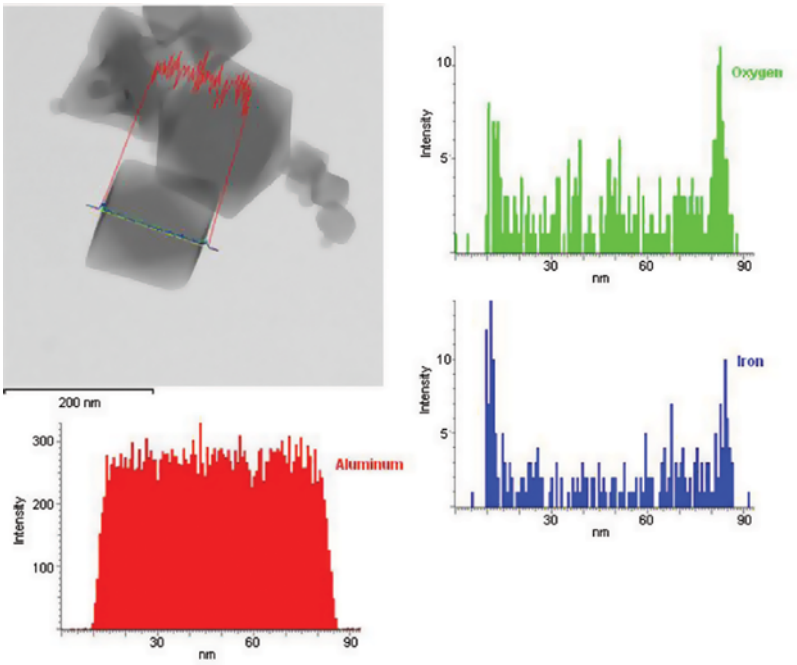

Figure 4. EDS line scan of a polyhedral aluminum particle from the iron coating experiment (color figure available online).

with literature data and no additional peaks are present that could indicate development of a mixed metal oxide.

Further analysis of the aluminum and aluminum oxide XPS peaks for this coated material compared to results from untreated aluminum revealed an unexpected result about the thickness of this layer. The relative peak heights in Fig. 5 for $Al:Al_2O_3$ compared to a previous result for uncoated synthesized Al show a much higher ratio for the uncoated case, indicating that the aluminum oxide layer was in fact larger for the iron oxide–coated case. Iron oxide coating on the aluminum

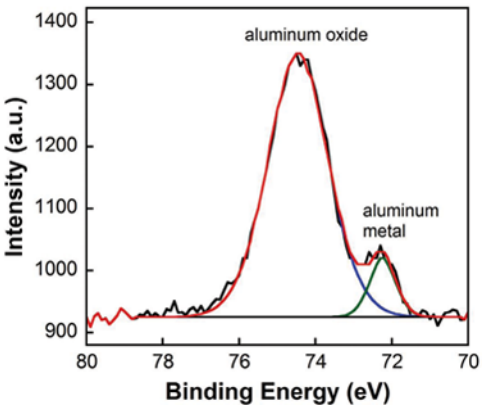

Figure 5. XPS results for iron oxide–coated Al nanoparticles (color figure available online).

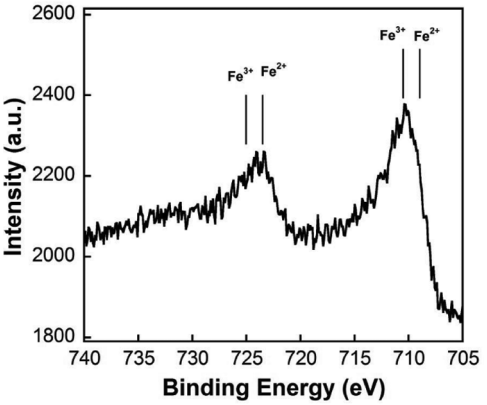

Figure 6. XPS results for iron in product particles.

surface thus was not passivated to prevent aluminum oxidation; it facilitated slightly increased aluminum oxidation. An understanding of metal oxides as an oxygen-lending agent makes this result sensible. At high temperatures, iron oxide will release oxygen that can be consumed by the bare aluminum. The iron oxide coating will continue taking up oxygen from the environment and passing it along to aluminum, thus growing an aluminum oxide shell, until this barrier becomes too large for oxygen to diffuse through. The heat released during the oxidation of iron may enable a deeper penetration of oxygen into the aluminum than in an uncoated case. For further examination of the iron oxide material on the surface, XPS results can be analyzed to determine the phase of the iron.

Analysis of Fig. 6 and comparison to XPS reference tables for iron phases revealed that the material on the particle surface was of the phase Fe_3O_4, iron (II, III) oxide [18], which formed during the low-temperature passivation with air.

In summary, information from XPS combined with EDS line scans led to the conclusion that we had a pure aluminum core with an Al_2O_3 shell surrounded by a Fe_3O_4 layer.

Reactivity Investigation

To examine the energetic properties, bulk product was collected from the iron oxide coating experiment on polypropylene membrane filters. For evaluation of the chemical impact caused by the coating during combustion, the material was combined with a stoichiometric amount of CuO from which a 25-mg sample was ignited and burned in a closed-volume combustion cell instrument with pressure and optical sensing. Details of this characterization method are shown elsewhere [19]. Three relevant pieces of information were obtained from these measurements: peak pressure, pressurization rate, and optical response. The latter two provide a qualitative measure of burn time, whereas the former provides a measure of the gas generation presumably from the oxygen release from oxide, a theory detailed by Zhou et al. for metastable intermolecular composites [20]. The burn time was evaluated as the full-width half-maximum of the optical response. Combustion tests were performed in the cell for stoichiometric thermite mixtures of uncoated

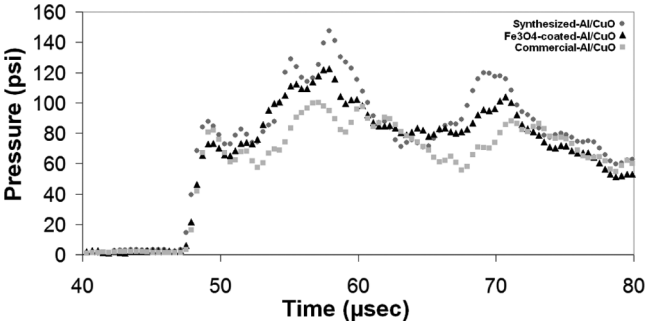

Figure 7. Pressure response from combustion tests of Fe_3O_4-coated Al compared to uncoated synthesized and commercial Al with stoichiometric CuO.

synthesized Al/CuO, Fe_3O_4-coated Al/CuO, and commercial Al/CuO. The commercial nanoaluminum consisted of spherical particles with an average size of 50 nm as reported by the supplier Argonide Corporation (Sanford, FL, USA) and confirmed by TEM inspection.

Figure 7 shows the temporal pressure response for a CuO-based stoichiometric thermite mixture of the uncoated and coated Al particles. The Fe_3O_4-coated Al/CuO combination showed a trend similar to that of the uncoated material with a slightly attenuated response. The maximum pressure values were 122 and 148 psi for coated and uncoated, respectively, with similar pressurization rates. Thus, the coating did not yield an enhanced reactivity in terms of pressure. This result can be explained by referencing the XPS results for the coated product in Fig. 5 showing an increased thickness of the aluminum oxide layer. The product had slightly lower fuel content and an increased barrier to reaction. It should be noted, however, that the Fe_3O_4-coated Al/CuO pressure cell result still showed a pressure response slightly higher than commercial nanoaluminum/CuO, which gives a maximum pressure of 100 psi.

Figure 8 shows the temporal optical response indicating a full-width half-maximum of 182 μs for Fe_3O_4-coated Al/CuO compared to 218 μs for uncoated synthesized Al/CuO and 224 μs for commercial nanoaluminum/CuO. This lower value for optical response full-width half-maximum suggests a faster overall burn time, but examination of the pressurization rate, the more important factor for an energetic

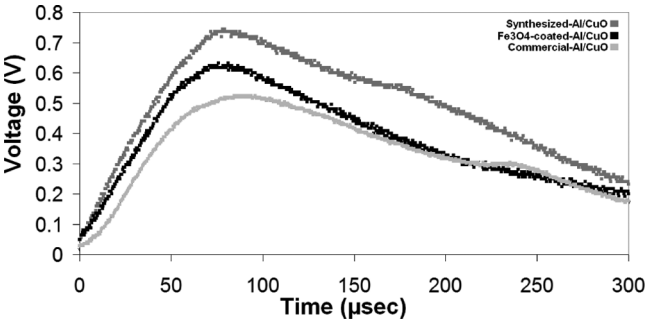

Figure 8. Optical response from combustion of Fe_3O_4-coated Al compared to synthesized and commercial Al with stoichiometric CuO.

application, did not show an enhancement for the coated case; a value of 11.8 psi/μs for the Fe_3O_4-coated aluminum/CuO compared to 13.7 psi/μs for the uncoated synthesized Al/CuO and 10.4 for commercial Al/CuO. Though the iron oxide–coated aluminum thermite may burn completely in a shorter total time, the rate at which maximum pressure is accomplished from the start of the event is similar to that of uncoated synthesized aluminum thermite. For comparison, uncoated synthesized aluminum was combined with commercial nanoFe_3O_4 along with stoichiometric CuO with ratios approximated to the amount of Al and Fe_3O_4 present in the coated sample. These ratios were calculated for a theoretical coating of 2 nm iron oxide on top of the aluminum oxide layer on a particle of bipyramidal shape. This material was then tested in the pressure cell, and the results are shown in Table 1.

The ignition temperate was determined from hot-wire T-jump measurements. Stoichiometric thermite samples were sonicated in hexane and deposited on a thin platinum wire for combustion. The experiment, fully detailed by Zhou et al. [21], employed a 76-μm-diameter platinum wire with a total heated length of ~12 mm that was replaced after each heating test. To ignite the sample, the wire was connected to a high-voltage power source that could be varied by changing the pulse voltage, resulting in heating rates of up to 5×10^5 K/s. Voltage and transient current through the circuit during the event were recorded, and using a wire resistance measurement real-time temperature information could be obtained throughout the event, allowing evaluation of temperature at the point of ignition. The results form these measurements are shown in Table 1, along with the pressure cell results.

T-jump ignition tests showed a decrease in critical ignition temperature for the Fe_3O_4-coated Al thermite case, a value of 973 K compared to 1076 K for the uncoated synthesized Al thermite. However, we note that the simple addition of Fe_3O_4 nanoparticles to Al/CuO did not show an increase in ignition temperature and thus it is clear that the addition of the iron oxide coat modified the transport rates of either aluminum or oxygen across the alumina coating. This is consistent with prior work by Andrzejak et al., who showed a decreased ignition temperature for millimeter-sized iron-coated aluminum particles caused by the formation of intermetallic Al-Fe alloys during combustion [7]. Because our particles were coated with iron oxide as opposed to pure iron, however, it cannot be assumed that the two materials follow similar reaction pathways. The route is more likely to be similar to that shown by La et al. for the formation of Fe_3Al by reaction of iron oxide with aluminum [8], though our case will be altered due to the Fe_3O_4 phase.

Table 1 Pressure cell results comparing commercial Al, Al(TibAl), Fe_3O_4-coated Al, and Al(TibAl) with nano-Fe_3O_4, all combined with stoichiometric CuO

Sample	Pressure rise (psi)	Pressurization rate (psi/μs)	Burn time (μs)	Ignition temperature (K)
Commercial Al/CuO	100.1	10.4	224.0	1,040
Al(TibAl)/CuO	147.5	13.7	218.0	1,076
Fe_3O_4-coated Al(TibAl)/CuO	122.5	11.8	182.0	973
Al(TibAl)/CuO + added nano-Fe_3O_4	142.6	14.3	215.2	1,112

Conclusions

This study presents an aerosol technique for production of an iron coating on bare nanoaluminum via gas-phase pyrolysis of iron pentacarbonyl. Subsequent air bleed to passivate iron is shown by XPS to completely oxidize the coating into Fe_3O_4. It was observed that the oxide thickness at the interface also included oxidation of aluminum. This added thickness is attributed to two causes: the Fe_3O_4 coating acting as a donor and iron oxidation heating the particle surface to increase the diffusivity of oxygen into the aluminum. Pressure cell combustion tests with a stoichiometric thermite mixture of Fe_3O_4-coated Al/CuO show a slightly lower pressure release compared to the uncoated case, which is attributed to the enlarged aluminum oxide layer formed during passivation. T-jump ignition tests for critical ignition temperature measurement of stoichiometric thermite mixtures reveal a lower value for the Fe_3O_4-coated case. This reduction could indicate an exothermic alloying reaction between aluminum and iron, as has been previously shown for iron-coated aluminum in the literature [6, 7].

Acknowledgments

Support for this work was provided by the Defense Threat Reduction Agency, the Army Research Office, and the University of Maryland Center for Energetic Concepts Development (CECD). We also gratefully acknowledge the support of the Maryland NanoCenter and its NispLab. The NispLab is supported in part by the NSF as an MRSEC Shared Experimental Facility.

References

[1] Piercey, D. G. and T. M. Klapotke. 2010. Nanoscale aluminum–metal oxide (thermite) reactions for application in energetic materials. *Central European Journal of Energetic Materials*, 7: 115–129.

[2] Hammerstroem, D. W., M. A. Burgers, S. W. Chung, E. A. Guliants, C. E. Bunker, K. M. Wentz, S. E. Hayes, S. W. Buckner, and P. A. Jelliss. 2011. Aluminum nanoparticles capped by polymerization of alkyl-substituted epoxides: Ratio-dependent stability and particle size. *Inorganic Chemistry*, 50: 5054–5059.

[3] Jouet, R. J., A. D. Warren, D. M. Rosenberg, V. J. Bellitto, K. Park, and M. R. Zachariah. 2005. Surface passivation of bare aluminum nanoparticles using perfluoroalkyl carboxylic acids. *Chemistry of Materials*, 17: 2987–2996.

[4] Horn, J. M., J. Lightstone, J. Carney, and J. Jouet. 2012. Preparation and characterization of functionalized aluminum nanoparticles. *American Institute of Physics Conference Proceedings*, 1426: 607–610.

[5] Breiter, A. L., V. M. Mal'tsev, and E. I. Popov. 1988. Means of modifying metallic fuel in condensed systems. *Combustion, Explosion and Shock Waves*, 26: 86–91.

[6] Shafirovich, E., P. E. Bocanegra, C. Chauveau, I. Gokalp, U. Goldshleger, V. Rosenband, and A. Gany. 2005. Ignition of single nickel-coated aluminum particles. *Proceedings of the Combustion Institute*, 30: 2055–2062.

[7] Andrzejak, T. A., E. Shafirovich, and A. Varma. 2008. Ignition of iron-coated and nickel-coated aluminum particles under normal- and reduced-gravity conditions. *Journal of Propulsion and Power*, 24: 805–813.

[8] La, P., J. Yang, D. J. H. Cockayne, W. Liu, Q. Xue, and Y. Li. 2006. Bulk nanocrystalline Fe_3Al-based material prepared by aluminothermic reaction. *Advanced Materials*, 18: 733–737.

[9] Kaplowitz, D. A., R. J. Jouet, and M. R. Zachariah. 2010. Aerosol synthesis and reactive behavior of faceted aluminum nanocrystals. *Journal of Crystal Growth*, 312: 3625–3630.

[10] Song, G. P., J. Bo, and R. Guo. 2004. The characterization and property of polystyrene compounding of α-Fe_2O_3 in the nano-scale. *Colloid and Polymer Science*, 282: 656–660.
[11] Kim, D. K., Y. Zhang, W. Voit, K. V. Rao, J. Kehr, B. Bjelke, and M. Muhammed. 2001. Superparamagnetic iron oxide nanoparticles for bio-medical applications. *Scripta Materialia*, 44: 1713–1717.
[12] Glavee, G. N., K. J. Klabunde, C. Sorensen, and G. C. Hadjipanayis. 1995. Chemistry of borohydride reduction of iron(II) and iron(III) ions in aqueous and nonaqueous media. Formation of nanoscale Fe, FeB and Fe2B powders. *Inorganic Chemistry*, 34: 28–35.
[13] Natter, H., M. Schmelzer, M. S. Loffler, C. E. Krill, A. Fitch, and R. Hempelmann. 2000. Grain-growth kinetics of nanocrystalline iron studied in situ by synchrotron real-time X-ray diffraction. *Journal of Physical Chemistry B*, 104: 2467–2476.
[14] Li, L., M. Fan, R. C. Brown, J. V. Leeuwen, J. Wang, W. Wang, Y. Song, and P. Zhang. 2006. Synthesis, properties, and environmental applications of nanoscale iron-based materials: A review. *Critical Reviews in Environmental Science and Technology*, 36: 405–431.
[15] Choi, C. J., X. L. Dong, and B. K. Kim. 2001. Characterization of Fe and Co nanoparticles synthesized by chemical vapor condensation. *Scripta Materialia*, 44: 2225–2229.
[16] Tepe, R. K., T. Jacksier, and R. M. Barnes. 1998. Determination of iron and nickel in electronic grade chlorine by sealed inductively coupled plasma atomic emission spectrometry. *Journal of Analytical Atomic Spectrometry*, 13: 989–994.
[17] Kim, S. H., K. S. Woo, B. Y. H. Liu, and M. R. Zachariah. 2005. Method of measuring charge distribution of nanosized aerosols. *Journal of Colloid and Interface Science*, 282: 46–57.
[18] Grosvenor, A. P., B. A. Kobe, M. C. Biesinger, and N. S. McIntyre. 2004. Investigation of multiplet splitting of Fe 2p XPS spectra and bonding in iron compounds. *Surface and Interface Analysis*, 36: 1564–1574.
[19] Sullivan, K. and M. R. Zachariah. 2010. Simultaneous pressure and optical measurements of nanoaluminum thermites: Investigating the reaction mechanism. *Journal of Propulsion and Power*, 26: 467–472.
[20] Zhou, L., N. Piekiel, S. Chowdhury, and M. R. Zachariah. 2010. Time-resolved mass spectrometry of the exothermic reaction between nanoaluminum and metal oxides: The role of oxygen release. *Journal of Physical Chemistry C*, 114: 14269–14275.
[21] Zhou, L., N. Piekiel, S. Chowdhury, and M. R. Zachariah. 2009. T-jump/time-of-flight mass spectrometry for time-resolved analysis of energetic materials. *Rapid Communications in Mass Spectrometry*, 23: 194–202.